# Quantifying the conceptual problems associated with the isotropic NICS through analyses of its underlying density

Acke, Guillaume; Van Damme, Sofie; Havenith, Remco W. A.; Bultinck, Patrick

*Published in:*
Physical Chemistry Chemical Physics

*DOI:*
10.1039/c8cp07343k



*Publication date:*
2019

PCCP

PAPER

View Article Online
View Journal | View Issue



Cite this: *Phys. Chem. Chem. Phys.*, 2019, **21**, 3145

# Quantifying the conceptual problems associated with the isotropic NICS through analyses of its underlying density

Guillaume Acke,[a] Sofie Van Damme,[a] Remco W. A. Havenith[b] and Patrick Bultinck*[a]

Received 29th November 2018,
Accepted 15th January 2019

DOI: 10.1039/c8cp07343k

rsc.li/pccp

The isotropic Nucleus Independent Chemical Shift ($NICS_{iso}$) is widely considered to be a suitable descriptor for aromaticity based on the correlations it exhibits with other aromaticity descriptors. To gain more insight into the origin of these correlations, we establish causal relations between the $NICS_{iso}$ and the underlying current density patterns by resolving the $NICS_{iso}$ into its underlying density. Our results indicate that the origin of the behavior of the $NICS_{iso}$ can be radically different from what is generally assumed. Not only does this bring into question the robustness of applying the $NICS_{iso}$ beyond the realms of where good correlations with other measures of aromaticity have been established, it also points to an inherent weakness in all interpretations of $NICS_{iso}$ values that are not based on additional data.



## 1 Introduction

The isotropic Nucleus Independent Chemical Shift ($NICS_{iso}$) was first proposed by Schleyer *et al.*[1] as a simple probe for "aromaticity". The $NICS_{iso}$ methodology (initially) entailed computing the magnetic shielding at ring centers – defined as the nonweighted mean of heavy atom coordinates – and assigning (anti)aromatic character based on the magnitude of the (positive) negative isotropic shift. The feasibility of this approach was justified using statistical correlations found within relatively limited sets of molecules, with other measures of aromaticity, such as the aromatic stabilization energy and magnetic susceptibility exaltations.[1,2] Aided in large part by its availability in standard quantum chemical packages, the $NICS_{iso}$ became *de facto* the most important method to judge the aromatic character of a system.[3–5]

Following its introduction, the $NICS_{iso}$ has been met with severe criticism,[6–14] most of which can be traced back to the fact that the $NICS_{iso}$ was substantiated with correlations with other aromaticity descriptors and not with causations in terms of the underlying current densities.[2,15] In this regard, important objections are that the $NICS_{iso}$ could consist of large local (primarily σ) contributions and that the $NICS_{iso}$ could capture more than only the aromatic ring currents, as these are primarily induced only by external magnetic fields perpendicular to the plane of the ring.

As an attempt to address these problems, Schleyer *et al.* proposed many refinements, including sampling the $NICS_{iso}$ at 1 Å above the ring centers[16] and refining the $NICS_{iso}$ to only the *zz*-component of the accompanying shielding tensor. Eventually, again based on statistical correlations, the $NICS^{\pi}_{zz}(0)$ was proposed as the method of choice for evaluating the π aromaticity of planar rings. Based on the conceptual problems associated with the "original" $NICS_{iso}$ (also termed $NICS_{iso}(0)$), the isotropic NICS was only recommended to obtain "rough indications of aromaticity" and should be used "with reservations".[2]

Not only is this advice frequently ignored, the limitations of the underlying statistical methodology are also frequently not recognized when the $NICS_{iso}$ methodology is adapted in new ways to complex systems. The reliance on correlations imposes that the same correlations have to be demonstrated for a set of systems representative for a new field of application before the $NICS_{iso}$ can be used as a proxy for the aromatic content of such systems. Furthermore, as the $NICS_{iso}$ alone cannot report what caused its value in terms of the underlying current density,[5] any additional interpretations beyond reporting the $NICS_{iso}$ values are problematic. As such, common statements such as "the maximum chemical shielding is found away from the ring center ... reflecting the π electron toroid densities"[1] or "local contributions fall of rapidly at points above the ring centers where the π contributions dominate"[2] have not been

[a] *Ghent Quantum Chemistry Group, Department of Chemistry, Krijgslaan 281, S3, B-9000 Ghent, Belgium. E-mail: Patrick.Bultinck@UGent.be*
[b] *Theoretical Chemistry, Zernike Institute for Advanced Materials and Stratingh Institute for Chemistry, University of Groningen, Groningen, AG, 9747, The Netherlands*

quantitatively substantiated and should be considered highly problematic.

Recently, based on work by Jameson and Buckingham,[17,18] and Lazzeretti *et al.*,[19–23] we have shown that by resolving the $NICS_{zz}$ in terms of space, sign and orbitals, these sources can be found and rendered quantitative[14] for the $NICS_{zz}$ descriptor. Using this methodology, we could quantitatively show that even the $NICS_{zz}$ has large local contributions and is prone to overinterpretations.

In light of these results for the $NICS_{zz}$, it is especially worrisome that despite the warnings of Schleyer more than ten years ago, the "original" $NICS_{iso}$ remains the most widely used descriptor to quantify aromaticity in planar systems, as evidenced by recent publications.[24–27] In order to gain more insight into the sources of $NICS_{iso}$ values, we will first extend the framework we recently introduced. Subsequently, we will apply it to the study of the $NICS_{iso}$ values associated with two prototypical aromatic systems: benzene and pyridine.

# 2 Methodology

## 2.1 Theory

As was shown by Lazzeretti and coworkers in the context of nuclear shieldings,[19–23] the density functions defined by Jameson and Buckingham[17,18] are useful to determine regions where shielding–deshielding mechanisms take place and to analyze the contribution by different domains of the current density. The NICSD methodology is based on resolving NICS quantities into such densities[14]

$$\mathrm{NICS}(\boldsymbol{r}_\mathrm{R}) = \int \mathrm{NICSD}(\boldsymbol{r};\boldsymbol{r}_\mathrm{R})\,\mathrm{d}\boldsymbol{r}, \tag{1}$$

and defining insightful descriptors derived from these densities. As such, we can define the isotropic Nucleus Independent Chemical Shift Density or $NICSD_{iso}$ associated with a reference position $\boldsymbol{r}_\mathrm{R}$ as

$$\mathrm{NICSD}_{\mathrm{iso}}(\boldsymbol{r};\boldsymbol{r}_\mathrm{R}) = -\frac{1}{3}\left[\Sigma_{xx}(\boldsymbol{r};\boldsymbol{r}_\mathrm{R}) + \Sigma_{yy}(\boldsymbol{r};\boldsymbol{r}_\mathrm{R}) + \Sigma_{zz}(\boldsymbol{r};\boldsymbol{r}_\mathrm{R})\right], \tag{2}$$

where $\boldsymbol{\Sigma}$ is the Jameson–Buckingham magnetic shielding density tensor field[21,28,29]

$$\Sigma_{\alpha\delta}(\boldsymbol{r};\boldsymbol{r}_\mathrm{R}) = -\frac{\mu_0}{4\pi}\varepsilon_{\alpha\beta\gamma}\frac{(r_{\mathrm{R}\beta} - r_\beta)}{\|\boldsymbol{r}_\mathrm{R} - \boldsymbol{r}\|^3}\mathscr{J}_\gamma^{B^{\mathrm{ext}},\delta}(\boldsymbol{r}), \tag{3}$$

with $\varepsilon_{\alpha\beta\gamma}$ the Levi-Civita tensor with implied Einstein summation, $\mu_0$ the permeability of free space and $\mathscr{J}_\gamma^{B^{\mathrm{ext}},\delta}(\boldsymbol{r})$ the $\gamma$-component of the current density tensor

$$\mathscr{J}_\gamma^{B^{\mathrm{ext}},\delta}(\boldsymbol{r}) = \frac{\partial}{\partial B_\delta^{\mathrm{ext}}}\boldsymbol{J}_\gamma^{\boldsymbol{B}^{\mathrm{ext}}}(\boldsymbol{r}). \tag{4}$$

By using generalized Dirac delta functions $\Delta$, we can define sign resolved $NICSD_{iso}$ fields

$$\mathrm{NICSD}_{\mathrm{iso}}^{-}(\boldsymbol{r};\boldsymbol{r}_\mathrm{R}) = \mathrm{NICSD}_{\mathrm{iso}}(\boldsymbol{r};\boldsymbol{r}_\mathrm{R})\Delta[\mathrm{NICSD}_{\mathrm{iso}}(\boldsymbol{r};\boldsymbol{r}_\mathrm{R}) < 0] \tag{5}$$

$$\mathrm{NICSD}_{\mathrm{iso}}^{+}(\boldsymbol{r};\boldsymbol{r}_\mathrm{R}) = \mathrm{NICSD}_{\mathrm{iso}}(\boldsymbol{r};\boldsymbol{r}_\mathrm{R})\Delta[\mathrm{NICSD}_{\mathrm{iso}}(\boldsymbol{r};\boldsymbol{r}_\mathrm{R}) > 0], \tag{6}$$

where $\Delta$ is only equal to one if the condition between square brackets is satisfied and is zero otherwise. These sign-resolved fields integrate to sign-resolved $NICS_{iso}$ values

$$\mathrm{NICS}_{\mathrm{iso}}^{\pm}(\boldsymbol{r}_\mathrm{R}) = \int \mathrm{NICSD}_{\mathrm{iso}}^{\pm}(\boldsymbol{r};\boldsymbol{r}_\mathrm{R})\mathrm{d}\boldsymbol{r}. \tag{7}$$

These sign-resolved $NICS_{iso}$ components sum to the $NICS_{iso}$

$$\mathrm{NICS}_{\mathrm{iso}}(\boldsymbol{r}_\mathrm{R}) = \mathrm{NICS}_{\mathrm{iso}}^{+}(\boldsymbol{r}_\mathrm{R}) + \mathrm{NICS}_{\mathrm{iso}}^{-}(\boldsymbol{r}_\mathrm{R}). \tag{8}$$

We can use such sign-resolved components to show that *e.g.* a negative $NICS_{iso}$ value

$$\mathrm{NICS}_{\mathrm{iso}}(\boldsymbol{r}_\mathrm{R}) < 0, \tag{9}$$

can consist of appreciable positive sign-resolved components, as long as this positive component is offset by an even larger negative sign-resolved component

$$-\mathrm{NICS}_{\mathrm{iso}}^{-}(\boldsymbol{r}_\mathrm{R}) > \mathrm{NICS}_{\mathrm{iso}}^{+}(\boldsymbol{r}_\mathrm{R}). \tag{10}$$

Any orbital decomposition (also called "dissection") of the current density can be echoed in the $NICSD_{iso}$ and the sign-resolved components defined above. For instance, the $NICSD_{iso}^{\pi}$ can be obtained by replacing the total current density tensor by the current density tensor uniquely associated with the $\pi$-system

$$\mathscr{J}_\gamma^{B^{\mathrm{ext}},\delta,\pi}(\mathbf{r}) = \sum_{n\in\pi}\mathscr{J}_\gamma^{B^{\mathrm{ext}},\delta,n}(\boldsymbol{r}). \tag{11}$$

## 2.2 Computational details

We fully optimized the geometry of benzene and pyridine at the Hartree–Fock level with the 6-311+g(d) basis set with Gaussian16,[30] followed by analytical frequency calculations to ensure a true minimum. We calculated the ipso-centric current density maps[31,32] at the coupled perturbed Hartree–Fock level in the 6-311g+(d) basis, using the GAMESS-UK package[33] linked to SYSMO.[34]

The resulting current density was expressed on a regular grid, centered on the ring center (nonweighted mean of the heavy atom coordinates), with a width of 12 a.u. and a step size of 1/12 a.u., in accordance with the fine grid implemented in the Gaussian16 standalone utility cubegen. All visualizations were obtained by interfacing with the Matplotlib Python package.[35]

The ipsocentric gauge distribution of the CTOCD-DZ method allows the total current density tensor to be decomposed as the sum of orbital contributions. For the aromatic systems we studied, three orbital-subsystems were taken into account: the inner shells (core), the σ system and the π system. According to Gajda *et al.*,[36] calculated NICS values of benzene depend on the method of calculation and the basis set quality to within only 1–3 ppm. Based on those results, the insights offered by the CTOCD-DZ method should also extend to other methods.

We note that all (non-orbital resolved) $NICSD_{\alpha\alpha}$-fields (with $\alpha \in \{x,y,z\}$) needed to construct the $NICSD_{iso}$ can also be obtained from Gaussian16 in Gaussian cube format by passing the

 

appropriate 'ShieldingDensity' keyword to the cubegen utility, which is included in Gaussian16.

# 3 Results and discussion

In this section, we apply the framework detailed in the methodology section to the study of benzene and pyridine. For this, we use the Z-scan methodology introduced by Stanger,[37] where the reference position is set at regular intervals along the *z*-axis. The orientation of the aromatic systems with respect to these axes is depicted in Fig. 1.

As the $NICSD_{iso}$-field is a three-dimensional scalar field, we visualize this field using several plotting planes, the orientation of which is illustrated in Fig. 2. In each cut-plane, each $NICSD_{iso}$ is visualized using a diverging colormap, with negative values in blue and positive values in red, where the maximum and minimum values are capped at 1 and $-1$ ppm respectively. To aid visualization, isocontour lines are also plotted at $\pm 10^n$ with $n \in \{3, 2, \ldots, -3, -4\}$.

## 3.1 Benzene

According to the observations of London, the "aromatic" character of planar unsaturated rings such as benzene manifests itself as an induced ring current under the influence of a uniform magnetic field perpendicular to the molecular plane.[38] An important criticism against the use of the $NICS_{iso}$ as an aromaticity descriptor is that the $NICS_{iso}$ measured at the ring center is not only affected by this ring current, but also by local circulations of σ-bond electrons, lone pairs and core electrons.

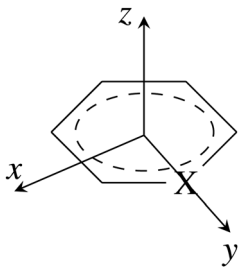


Fig. 1 Orientation of the *x*, *y*, and *z* axis relative to the aromatic systems, with X a carbon (benzene) or nitrogen (pyridine) atom.

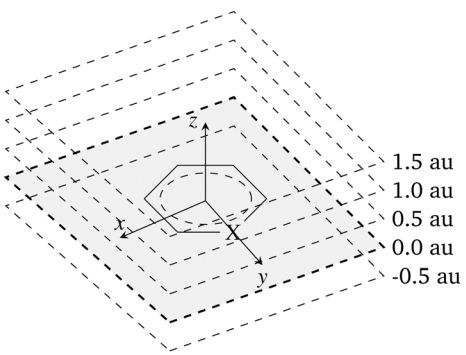


Fig. 2 Orientation of the cut planes through the $NICSD_{iso}$ fields.

Initially, Schleyer suggested that the height of the NICS probe should be increased to 1 Å, where the local contributions were believed to be diminished relative to the ring current effects.[16,39]

At first sight, the Z-scan of the orbital-resolved $NICS_{iso}$ shown in Fig. 3(a) seems to support such reasoning. The $NICS^{\sigma}_{iso}$ rapidly drops in magnitude and is negligible around 1 Å. This rapid drop was taken to indicate that σ contributions are short ranged.[2] Furthermore, as the cores have a negligible contribution at all heights, the $NICS^{\pi}_{iso}$ becomes equal to the $NICS_{iso}$ around 1 Å. According to Schleyer, these nearly identical values indicate that $NICS_{iso}(1)$ can be used as a proxy for the $NICS^{\pi}_{iso}(1)$.[16] The cause of this behavior was attributed to the fact that the π orbitals have their maximum density around 1 Å.[3]

However, the Z-scan of the sign-resolved orbital contributions shown in Fig. 3(b) indicates that the σ contributions are not short-ranged. Instead, the drop in $NICS^{\sigma}_{iso}$ is a consequence of the sign-resolved σ contributions becoming equal in magnitude (but opposite in sign). Furthermore, the negative contribution of the σ framework actually becomes larger than the negative π contributions beyond 2.5 a.u. Consequently, although the $NICS_{iso}$ and the $NICS^{\pi}_{iso}$ are equal around 1 Å, the cause of these similar values is not the same, as the $NICS_{iso}$ consists of all contributions (σ, π and core). In contrast to the statements of Schleyer,[15] the $NICS_{iso}$ does not reflect the π electron toroid densities above the ring centers, as beyond 2.5 a.u. the σ framework has both the largest positive and negative shift contributions. As such, although their values may be the same for benzene, it is not substantiated that the $NICS_{iso}$ can always be used as a proxy for the $NICS^{\pi}_{iso}$.

The sign-resolved plots in Fig. 3(b) also indicate that the negligible $NICS^{core}_{iso}$ is in fact hiding significant sign-resolved core contributions, that gradually decay with increasing probe height. As such, one has to take into account that a negligible $NICS_{iso}$-value can hide significant contributions.

In contrast to the $NICS^{\pi}_{zz}$,[14] the $NICS^{\pi}_{iso}$ has positive shift contributions, that achieve a maximum around 1 Å. As such, a negative $NICS_{iso}$ contribution can consist of appreciable positive sign-resolved components, that are offset by even larger negative components.

We can gain more insight into the behavior of these sign-resolved components by inspecting the respective NICSD fields shown in Fig. 4. Although these fields are associated with the prototypical aromatic molecule benzene, they do not exhibit a topology that can be qualitatively matched with any model for aromatic systems. In this respect, the NICSD contributions in the nodal plane are especially problematic, as they prohibit any explanation in terms of a toroidal model. Thus, although the NICS may exhibit good correlations with other descriptors for aromaticity, it is based on fields that have little to no features chemists normally associate with aromatic systems.

We also note that the topology of the $NICSD_{iso}$ is more similar to the $NICSD^{\sigma}_{iso}$ than that of the $NICSD^{\pi}_{iso}$. Furthermore, increasing the height of the probe also increases the similarity between the $NICSD_{iso}$ and the $NICSD^{\sigma}_{iso}$. These plots show that,

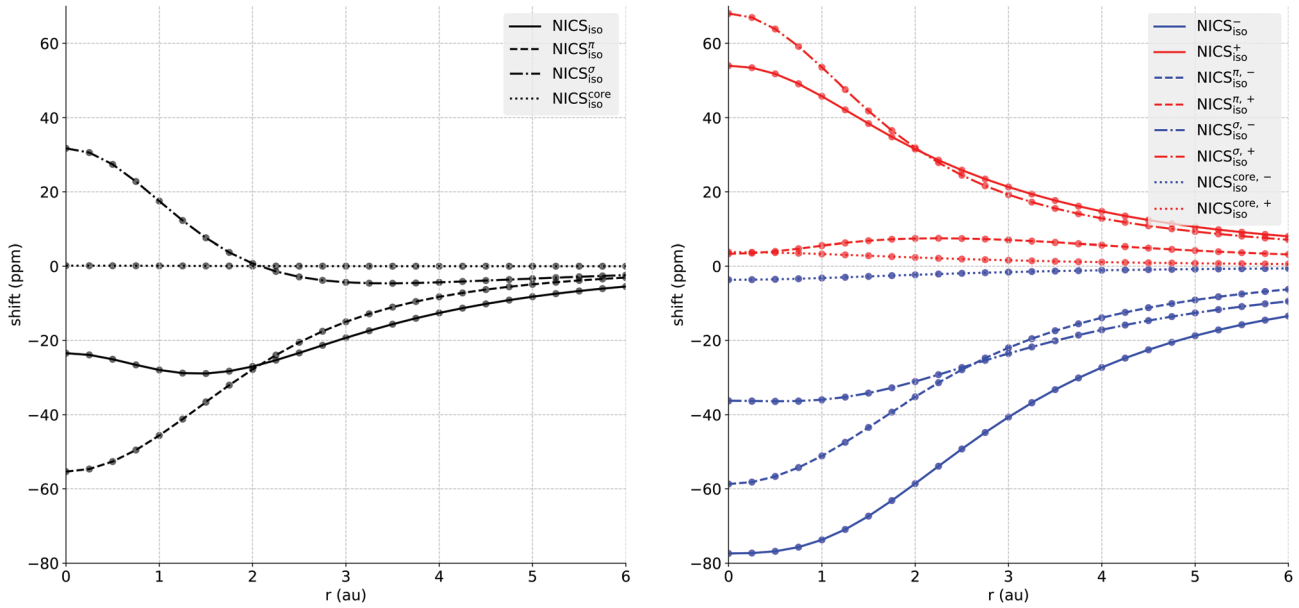


(a) Orbital resolved. (b) Orbital and sign resolved.

Fig. 3 Z-scan of the $NICS_{iso}$ for benzene with reference points sampled at $\boldsymbol{r}_R = (0.0,0.0,r_{Rz})$.

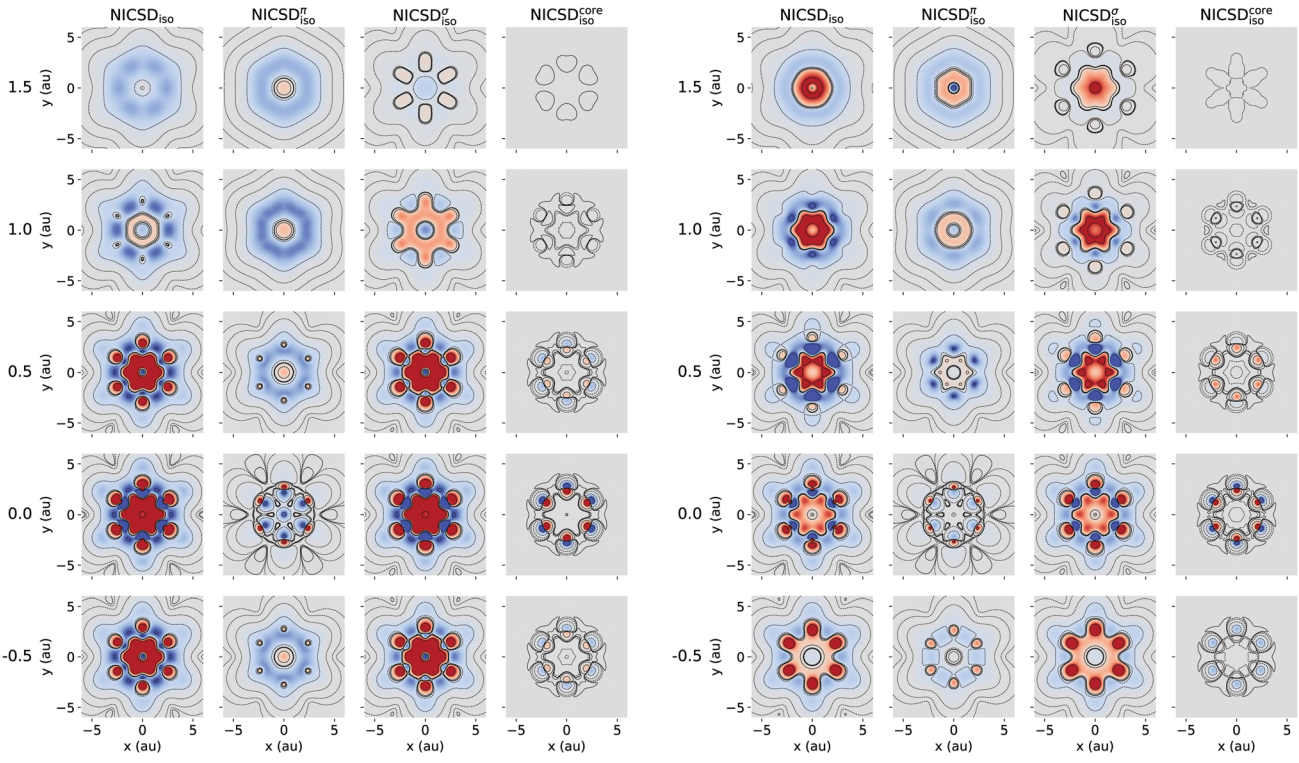


(a) $\boldsymbol{r}_R = (0.0, 0.0, 0.0)$ (au) (b) $\boldsymbol{r}_R = (0.0, 0.0, 2.0)$ (au)

Fig. 4 Collection of cut planes at $r_z = -0.5$, 0.0, 0.5, 1.0 and 1.5 a.u., through the $NICSD_{iso}$ field and the orbital resolved $NICSD_{iso}$ fields of benzene, associated with probes positioned along the $z$-axis at $(0,0,r_{Rz})$ with $r_{Rz}$ equal to 0.0 or 2.0 a.u. respectively. Blue regions indicate negative shielding contributions, whereas red regions indicate positive shielding contributions. Dashed contour lines denote negative values, solid contour lines positive values. Contour values are plotted at $\pm 10^n$ with $n \in \{3, 2, \ldots, -3, -4\}$.

although the $NICS^{\sigma}_{iso}$ contribution drops to zero and the $NICS_{iso}$ is equal to the $NICS^{\pi}_{iso}$ at 2 a.u., the underlying shift density patterns that cause these values are completely different.

We can reduce the complexity of the $NICSD_{iso}$ plots by integrating over "slices" of space, with each slice a rectangular volume parallel to the $xy$-plane with a thickness of $\Delta = 1/12$ a.u.

 

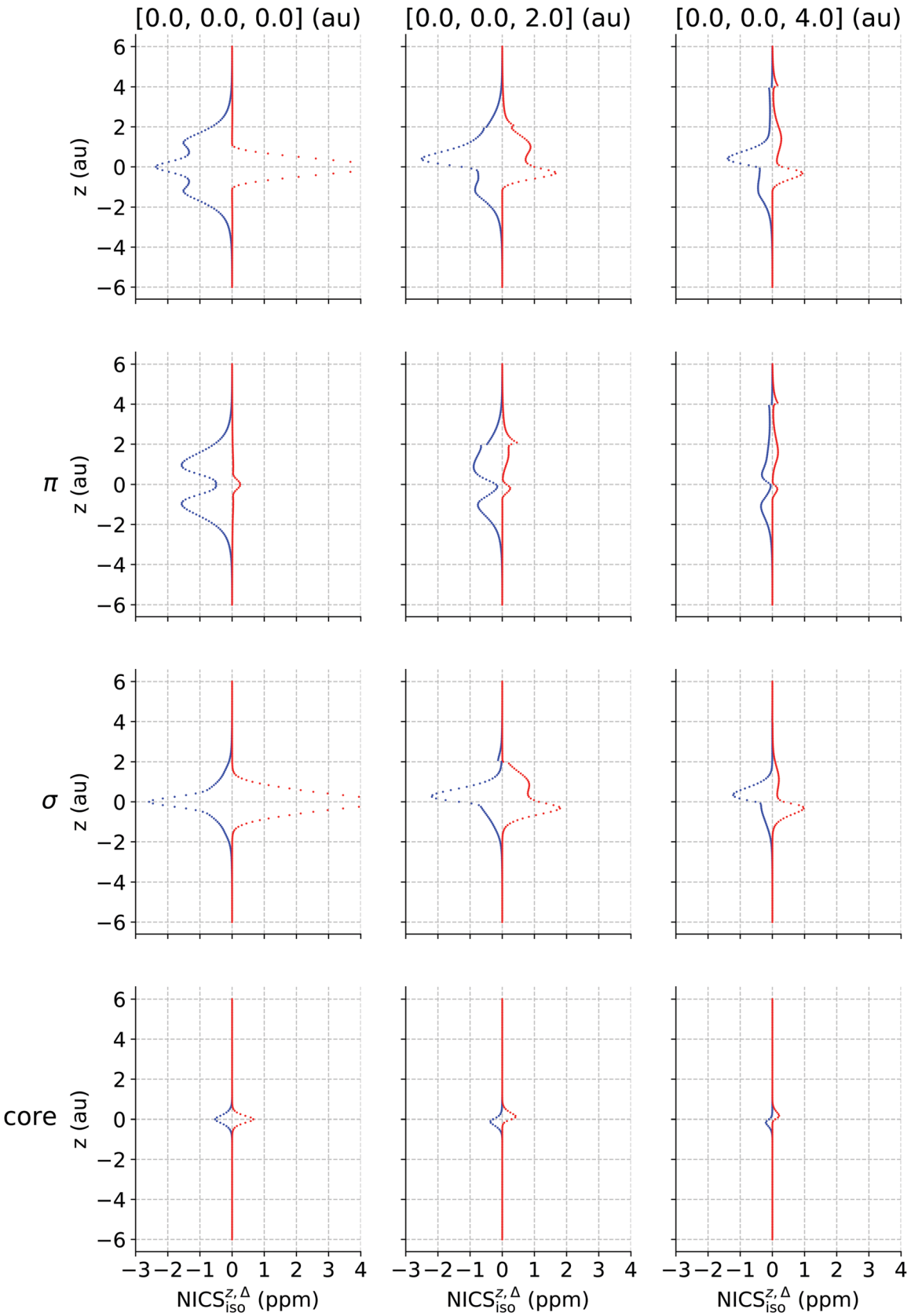


Fig. 5 The NICS$^{z,\Delta}_{iso}(h)$ shift contributions of benzene for non-overlapping slices parallel to the *xy*-plane at a height *h* with a thickness of $\Delta$ = 1/12 a.u., centered on regularly spaced points with an interval of 1/12 a.u. At each height *h*, the contributions are sign-resolved into negative (blue) and positive (red) contributions. The $\boldsymbol{r}_R$ coordinates of the probes are given in the respective headings.

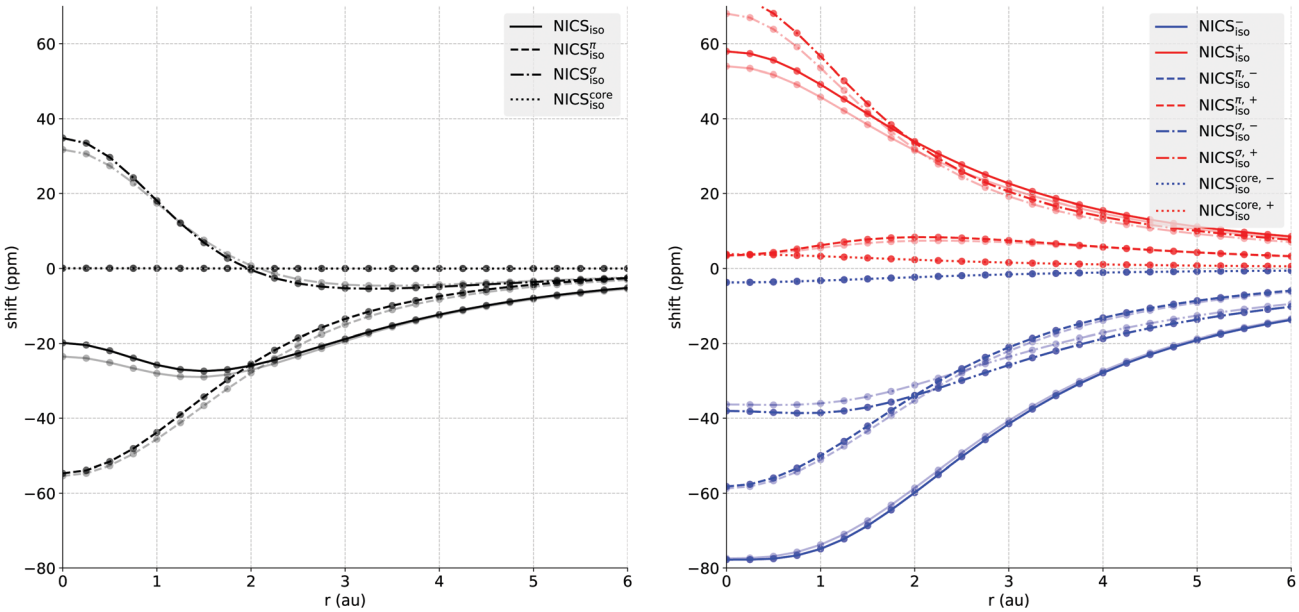


(a) Orbital resolved. (b) Orbital and sign resolved.

**Fig. 6** Z-scan of the NICS$_{iso}$ for pyridine with reference points sampled at $\boldsymbol{r}_R$ = (0.0,0.0,$r_{Rz}$). The corresponding values for benzene are overlayed in a lighter color.

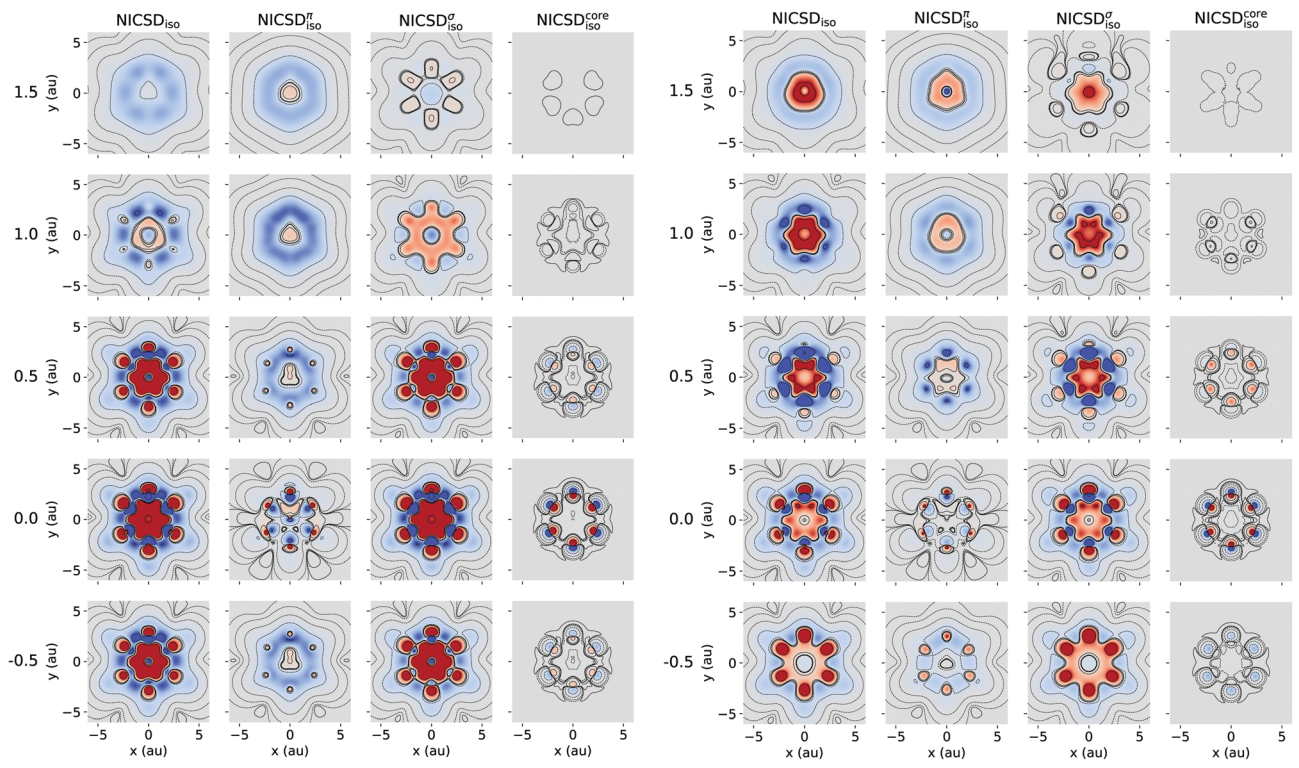


(a) $\boldsymbol{r}_R$ = (0.0, 0.0, 0.0) (au) (b) $\boldsymbol{r}_R$ = (0.0, 0.0, 2.0) (au)

**Fig. 7** Collection of cut planes at $r_z$ = −0.5, 0.0, 0.5, 1.0 and 1.5 a.u., through the NICSD$_{iso}$ field and the orbital resolved NICSD$_{iso}$ fields of pyridine, associated with probes positioned along the $z$-axis at (0,0,$r_{Rz}$) with $r_{Rz}$ equal to 0.0 or 2.0 a.u. respectively. Blue regions indicate negative shielding contributions, whereas red regions indicate positive shielding contributions. Dashed contour lines denote negative values, solid contour lines positive values. Contour values are plotted at $\pm 10^i$ with $i \in \{3, 2, \ldots, -3, -4\}$.

 

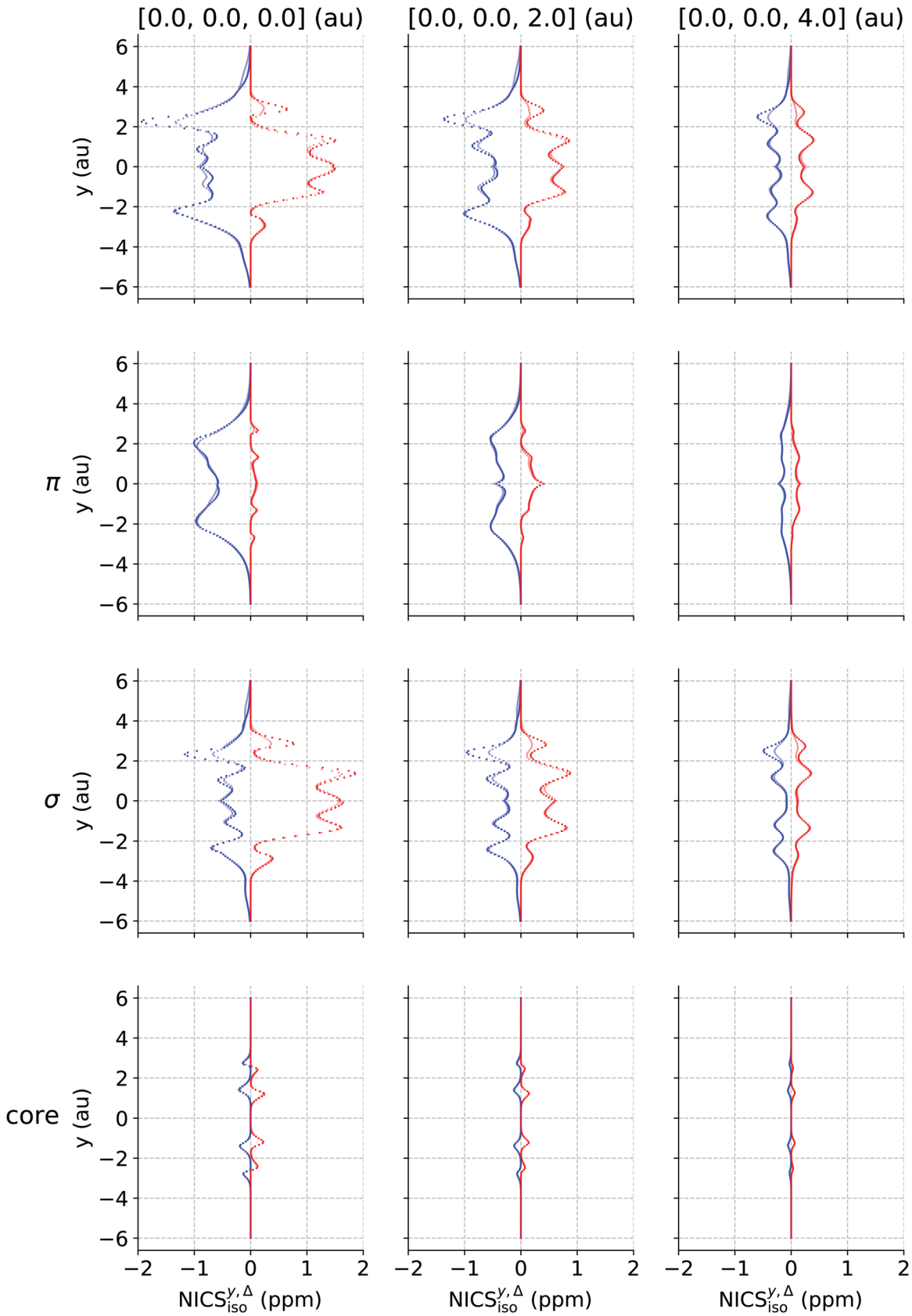


Fig. 8 The NICS$^{y,\Delta}_{iso}(h)$ shift contributions of pyridine for non-overlapping slices parallel to the $xz$-plane at a height $h$ with a thickness of $\Delta$ = 1/12 a.u., centered on regularly spaced points with an interval of 1/12 a.u. At each height $h$, the contributions are sign-resolved into negative (blue) and positive (red) contributions. The $\boldsymbol{r}_R$ coordinates of the probes are given in the respective headings. The corresponding values for benzene are overlayed in a lighter color.

As such, the shift contribution $\mathrm{NICS}^{z,\Delta}_{\mathrm{iso}}(h)$ of such a slice at a given height $h$ is given by

$$\mathrm{NICS}^{z,\Delta}_{\mathrm{iso}}(h) = \int_{h-\frac{\Delta}{2}}^{h+\frac{\Delta}{2}} \mathrm{d}\boldsymbol{r}_z \int_{-\infty}^{+\infty} \mathrm{d}\boldsymbol{r}_x \int_{-\infty}^{+\infty} \mathrm{d}\boldsymbol{r}_y \mathrm{NICSD}_{\mathrm{iso}}(\boldsymbol{r};\boldsymbol{r}_{\mathrm{R}}). \quad (12)$$

If we divide space into such nonoverlapping slices, centered at evenly spaced positions with an interval of 1/12 a.u., we obtain the results plotted in Fig. 5. These plots confirm that, although the $\mathrm{NICS}^{\sigma}_{\mathrm{iso}}$ contribution drops to zero, increasing the height of the probe increases the correspondence between the $\mathrm{NICS}_{\mathrm{iso}}$ and the $\mathrm{NICS}^{\sigma}_{\mathrm{iso}}$. As such, the $\mathrm{NICS}_{\mathrm{iso}}$ should not be used a proxy for the $\mathrm{NICS}^{\pi}_{\mathrm{iso}}$, and even more so at larger heights.

### 3.2 Pyridine

The main idea behind NICS methodologies is that a difference in NICS values can be associated with a difference in ''aromaticity''. In prototypical aromatic molecules such as pyridine and benzene, this aromaticity can uniquely be associated with the properties of the π system. As such, for this central idea to hold, the difference in NICS values should be largely due to changes in the contributions of the respective π systems.

Based on the $\mathrm{NICS}_{\mathrm{iso}}$ Z-scan of pyridine overlayed with the Z-scan of benzene in Fig. 6(a), pyridine should be considered less aromatic than benzene. Although the $\mathrm{NICS}_{\mathrm{iso}}$ of pyridine is less negative than the $\mathrm{NICS}_{\mathrm{iso}}$ of benzene at the ring center, the $\mathrm{NICS}^{\pi}_{\mathrm{iso}}$ values are equal. Traditionally, this was taken to indicate that at this height, the difference in $\mathrm{NICS}_{\mathrm{iso}}$ values was contaminated by changes in the σ framework.[2] At 2 a.u., the $\mathrm{NICS}^{\sigma}_{\mathrm{iso}}$ for both pyridine and benzene are approximately equal to zero, and the difference in $\mathrm{NICS}_{\mathrm{iso}}$ can be largely equated to the difference in $\mathrm{NICS}^{\pi}_{\mathrm{iso}}$. Again, this is commonly believed to support the reasoning that sampling at larger heights is to be preferred.

Although the $\mathrm{NICS}^{\sigma}_{\mathrm{iso}}$ of pyridine is larger at the ring center, it drops faster with increasing height than the corresponding $\mathrm{NICS}^{\sigma}_{\mathrm{iso}}$ of benzene, eventually becoming even smaller in magnitude than the $\mathrm{NICS}^{\sigma}_{\mathrm{iso}}$ of benzene. However, the sign-resolved contributions in Fig. 6(b) indicate that in the case of pyridine, all $\mathrm{NICS}^{\sigma}_{\mathrm{iso}}$ are larger in magnitude than the $\mathrm{NICS}^{\sigma}_{\mathrm{iso}}$ contributions for benzene. This indicates that only the balance between positive and negative shift components is changed with increasing height of the reference probe; the change in $\mathrm{NICS}_{\mathrm{iso}}$ does not show that the influence of the σ framework of pyridine declines faster than that of benzene. At a height of 2 a.u., that balance is shifted in such a way that the $\mathrm{NICS}^{\sigma}_{\mathrm{iso}}$ for both systems is approximately zero. Again, this does not signify that at this height the σ framework no longer plays any role in the $\mathrm{NICS}_{\mathrm{iso}}$ value.

We can gain more insight into this behavior by comparing the $\mathrm{NICSD}_{\mathrm{iso}}$ fields of pyridine shown in Fig. 7 to the $\mathrm{NICSD}_{\mathrm{iso}}$ fields of benzene shown in Fig. 4. We again note that the $\mathrm{NICSD}_{\mathrm{iso}}$ field is mainly influenced by contributions of the $\mathrm{NICSD}^{\sigma}_{\mathrm{iso}}$ field. In general, the $\mathrm{NICSD}^{\pi}_{\mathrm{iso}}$ field reflects the influence of the more electronegative nitrogen atom, that attracts shift density towards itself. However, the $\mathrm{NICSD}^{\sigma}_{\mathrm{iso}}$ field also exhibits similar changes in its current density patterns.

Again, we can integrate over ''slices'' of space to reduce the complexity contained in the $\mathrm{NICSD}_{\mathrm{iso}}$ plots. In this case, we integrate over rectangular volumes parallel to the *xz*-plane with a thickness of $\Delta = 1/12$ a.u. As such, the shift contribution $\mathrm{NICS}^{y,\Delta}_{\mathrm{iso}}(h)$ at a distance of $h$ along the *y*-axis (as oriented in Fig. 1) is given by

$$\mathrm{NICS}^{y,\Delta}_{\mathrm{iso}}(h) = \int_{h-\frac{\Delta}{2}}^{h+\frac{\Delta}{2}} \mathrm{d}\boldsymbol{r}_y \int_{-\infty}^{+\infty} \mathrm{d}\boldsymbol{r}_x \int_{-\infty}^{+\infty} \mathrm{d}\boldsymbol{r}_z \ \mathrm{NICSD}_{\mathrm{iso}}(\boldsymbol{r};\boldsymbol{r}_{\mathrm{R}}). \quad (13)$$

If we divide space into such nonoverlapping slices, centered at evenly spaced positions with an interval of 1/12 a.u., we obtain the results plotted in Fig. 8. At the ring center, the negative $\mathrm{NICS}^{y,\Delta}_{\mathrm{iso}}$ contributions indicate that the higher density around the nitrogen atom is offset by a concommitant decrease in density around the meta and para carbon atoms. After summation over the sign-resolved contributions, this delicate balance leads to a negligible difference in $\mathrm{NICS}^{\pi}_{\mathrm{iso}}$ values at the ring center. By moving to 2 a.u., this balance is disturbed in favor of a total lower $\mathrm{NICS}^{\pi}_{\mathrm{iso}}$ for benzene. However, the underlying field no longer exhibits the same topology: the nitrogen atom no longer has a larger density associated with itself and the positive contributions lie mainly in the center of the ring. Hence, although moving to larger heights increases the distance between the $\mathrm{NICS}^{\pi}_{\mathrm{iso}}$ of benzene and pyridine, the underlying field indicates that is not caused by regions traditionally associated with ''aromaticity''.

These plots also confirm that the $\mathrm{NICS}_{\mathrm{iso}}$ itself is largely based on contributions from the σ framework; the effects of the π system are largely indiscernible at 2 a.u. As such, although the difference in the respective $\mathrm{NICS}_{\mathrm{iso}}$ of pyridine and benzene may be equal to the difference in $\mathrm{NICS}^{\pi}_{\mathrm{iso}}$ at 2 a.u., its underlying causes are completely different. As the influence of the π system is minor in comparison the σ system, these findings question whether a difference in $\mathrm{NICS}_{\mathrm{iso}}$ values actually represents a difference in aromatic character. As such, these results show that the $\mathrm{NICS}_{\mathrm{iso}}$, as an isotropic magnetic criterion, is indeed influenced, and even dominated, by effects other than ''aromaticity'', and that the $\mathrm{NICS}_{\mathrm{iso}}$ ''is measuring different things'', a possibility that Schleyer already warned about more than ten years ago.[2]

## 4 Conclusions

The $\mathrm{NICS}_{\mathrm{iso}}$ is commonplace in computational chemistry as an aromaticity index, despite the warning issued by Schleyer more than ten years ago that ''the conceptual imperfections of all isotropic NICS indexes should be recognized''.[2] In this study, we have shown that although the $\mathrm{NICS}_{\mathrm{iso}}$ may be able to correlate well with other measures of aromaticity for a limited portion of chemical space, there is no underlying causal reason why this should be the case in general. This indicates that for each area of application, the existence of such correlations has to be established before the $\mathrm{NICS}_{\mathrm{iso}}$ can be used as a proxy for ''aromaticity''. Furthermore, it also shows that any interpretations of the resulting $\mathrm{NICS}_{\mathrm{iso}}$ values that are not backed by additional data are highly prone to misinterpretation.

 

Now that the $NICS_{iso}$ is increasingly being used in ways that reach far beyond the applications for which the $NICS_{iso}$ was originally intended,[40,41] further research into the causes why the $NICS_{iso}$ is able to exhibit the good correlations reported is urgently needed. Furthermore, such research should be supplemented with critical investigations of the interpretations reported for systems where such correlations have not been established.

## Conflicts of interest

There are no conflicts to declare.

## References

1 P. R. von Schleyer and H. Jiao, *Pure Appl. Chem.*, 1996, **68**, 209–218.
2 H. Fallah-Bagher-Shaidaei, C. S. Wannere, C. Corminboeuf, R. Puchta and P. v. R. Schleyer, *Org. Lett.*, 2006, **8**, 863–866.
3 Z. Chen, C. S. Wannere, C. Corminboeuf, R. Puchta and P. v. R. Schleyer, *Chem. Rev.*, 2005, **105**, 3842–3888.
4 R. Islas, T. Heine and G. Merino, *Acc. Chem. Res.*, 2011, **45**, 215–228.
5 R. Gershoni-Poranne and A. Stanger, *Chem. Soc. Rev.*, 2015, **44**, 6597–6615.
6 P. Lazzeretti, *Prog. Nucl. Magn. Reson. Spectrosc.*, 2000, **36**, 1–88.
7 J. Gomes and R. Mallion, *Chem. Rev.*, 2001, **101**, 1349–1384.
8 J. I. Aihara, *Chem. Phys. Lett.*, 2002, **365**, 34–39.
9 P. Lazzeretti, *Phys. Chem. Chem. Phys.*, 2004, **6**, 217–223.
10 J. Poater, M. Solà, R. G. Viglione and R. Zanasi, *J. Org. Chem.*, 2004, **69**, 7537–7542.
11 S. Pelloni, G. Monaco, P. Lazzeretti and R. Zanasi, *Phys. Chem. Chem. Phys.*, 2011, **13**, 20666–20672.
12 S. Pelloni and P. Lazzeretti, *J. Phys. Chem. A*, 2011, **115**, 4553–4557.
13 S. Van Damme, G. Acke, R. W. Havenith and P. Bultinck, *Phys. Chem. Chem. Phys.*, 2016, **18**, 11746–11755.
14 G. Acke, S. Van Damme, R. W. Havenith and P. Bultinck, *J. Comput. Chem.*, 2018, **39**, 511–519.
15 P. v. R. Schleyer, C. Maerker, A. Dransfeld, H. Jiao and N. J. van Eikema Hommes, *J. Am. Chem. Soc.*, 1996, **118**, 6317–6318.
16 P. von Ragué Schleyer, M. Manoharan, Z.-X. Wang, B. Kiran, H. Jiao, R. Puchta and N. J. van Eikema Hommes, *Org. Lett.*, 2001, **3**, 2465–2468.
17 C. J. Jameson and A. Buckingham, *J. Chem. Phys.*, 1979, **83**, 3366–3371.
18 C. J. Jameson and A.-D. Buckingham, *J. Chem. Phys.*, 1980, **73**, 5684–5692.
19 A. Soncini, P. Fowler, P. Lazzeretti and R. Zanasi, *Chem. Phys. Lett.*, 2005, **401**, 164–169.
20 S. Pelloni and P. Lazzeretti, *Theor. Chem. Acc.*, 2007, **118**, 89–97.
21 I. G. Cuesta, D. Merás, A. Sánchez, S. Pelloni and P. Lazzeretti, *J. Comput. Chem.*, 2009, **30**, 551–564.
22 P. Lazzeretti, *Electronic current density induced by magnetic fields and nuclear magnetic dipoles: theory and computation of NMR spectral parameters*, Elsevier, 2013, vol. 3.
23 P. Lazzeretti, *Applications of Topological Methods in Molecular Chemistry*, Springer, 2016, pp. 151–226.
24 H. Peng, P. Huang, P. Yi, F. Xu and L. Sun, *J. Mol. Struct.*, 2018, **1154**, 590–595.
25 Y. Deng, D. Yu, X. Cao, L. Liu, C. Rong, T. Lu and S. Liu, *Mol. Phys.*, 2018, **116**, 956–968.
26 C. Sah, A. K. Yadav and S. Venkataramani, *J. Phys. Chem. A*, 2018, **122**, 5464–5476.
27 X.-S. Ke, Y. Hong, V. M. Lynch, D. Kim and J. L. Sessler, *J. Am. Chem. Soc.*, 2018, **140**, 7579–7586.
28 M. Ferraro, P. Lazzeretti, R. Viglione and R. Zanasi, *Chem. Phys. Lett.*, 2004, **390**, 268–271.
29 M. B. Ferraro, F. Faglioni, A. Ligabue, S. Pelloni and P. Lazzeretti, *Magn. Reson. Chem.*, 2005, **43**, 316–320.
30 M. J. Frisch, G. W. Trucks, H. B. Schlegel, G. E. Scuseria, M. A. Robb, J. R. Cheeseman, G. Scalmani, V. Barone, G. A. Petersson, H. Nakatsuji, X. Li, M. Caricato, A. V. Marenich, J. Bloino, B. G. Janesko, R. Gomperts, B. Mennucci, H. P. Hratchian, J. V. Ortiz, A. F. Izmaylov, J. L. Sonnenberg, D. Williams-Young, F. Ding, F. Lipparini, F. Egidi, J. Goings, B. Peng, A. Petrone, T. Henderson, D. Ranasinghe, V. G. Zakrzewski, J. Gao, N. Rega, G. Zheng, W. Liang, M. Hada, M. Ehara, K. Toyota, R. Fukuda, J. Hasegawa, M. Ishida, T. Nakajima, Y. Honda, O. Kitao, H. Nakai, T. Vreven, K. Throssell, J. A. Montgomery, Jr., J. E. Peralta, F. Ogliaro, M. J. Bearpark, J. J. Heyd, E. N. Brothers, K. N. Kudin, V. N. Staroverov, T. A. Keith, R. Kobayashi, J. Normand, K. Raghavachari, A. P. Rendell, J. C. Burant, S. S. Iyengar, J. Tomasi, M. Cossi, J. M. Millam, M. Klene, C. Adamo, R. Cammi, J. W. Ochterski, R. L. Martin, K. Morokuma, O. Farkas, J. B. Foresman and D. J. Fox, *Gaussian 16 Revision A.03*, 2016, Gaussian Inc., Wallingford CT.
31 P. Lazzeretti, M. Malagoli and R. Zanasi, *Chem. Phys. Lett.*, 1994, **220**, 299–304.
32 E. Steiner and P. W. Fowler, *J. Phys. Chem. A*, 2001, **105**, 9553–9562.
33 M. F. Guest, I. J. Bush, H. J. J. Van Dam, P. Sherwood, J. M. H. Thomas, J. H. Van Lenthe, R. W. A. Havenith and J. Kendrick, *Mol. Phys.*, 2005, **103**, 719–747.
34 P. Lazzeretti and R. Zanasi, *SYSMO Package (University of Modena)*, Additional routines for evaluation and plotting of current density by E. Steiner, P. Fowler, R. W. A. Havenith and A. Soncini, 1980.
35 J. D. Hunter, *Comput. Sci. Eng.*, 2007, **9**, 90–95.
36 Ł. Gajda, T. Kupka, M. A. Broda, M. Leszczyńska and K. Ejsmont, *Magn. Reson. Chem.*, 2018, **56**, 265–275.
37 A. Stanger, *J. Org. Chem.*, 2006, **71**, 883–893.
38 F. London, *J. Phys.*, 1937, **8**, 397–409.
39 P. v. R. Schleyer, H. Jiao, N. J. v. E. Hommes, V. G. Malkin and O. L. Malkina, *J. Am. Chem. Soc.*, 1997, **119**, 12669–12670.
40 E. Kleinpeter, S. Klod and A. Koch, *THEOCHEM*, 2007, **811**, 45–60.
41 P. B. Karadakov and K. E. Horner, *J. Chem. Theory Comput.*, 2016, **12**, 558–563.